The effects of pressure on the electronic, transport and dynamical properties of AuX_2 (X = Al, Ga and In)

2007 J. Phys.: Condens. Matter 19 425224

(http://iopscience.iop.org/0953-8984/19/42/425224)

IOP PUBLISHING JOURNAL OF PHYSICS: CONDENSED MATTER

J. Phys.: Condens. Matter **19** (2007) 425224 (13pp) doi:10.1088/0953-8984/19/42/425224

The effects of pressure on the electronic, transport and dynamical properties of AuX_2 (X = Al, Ga and In)

Q Li, Y Li, T Cui, Y Wang, L J Zhang, Y Xie, Y L Niu, Y M Ma[1] and G T Zou

National Laboratory of Superhard Materials, Jilin University, Changchun 130012, People's Republic of China

E-mail: mym@jlu.edu.cn

Received 3 August 2007
Published 18 September 2007
Online at stacks.iop.org/JPhysCM/19/425224

Abstract

The electronic band structure, transport properties, and lattice dynamics in AuX_2 (X = Al, Ga and In) under high pressure have been extensively studied with full potential linearized augmented plane wave and pseudopotential plane wave methods. The theoretical results for the electronic band structure and Fermi surface reveal pressure-induced electronic topological transitions (ETTs) in $AuGa_2$ and $AuIn_2$, while they are absent in $AuAl_2$, in excellent agreement with the experimental observations. Moreover, calculations of the transport properties at different pressures reveal subtle changes in the band structure close to the Fermi surface of the three intermetallic compounds. It is clear that the anomalies in transport properties are due to ETTs. Interestingly, a pressure-induced soft transverse acoustic (TA) phonon mode is identified only in $AuGa_2$. The TA phonon instability at the Brillouin zone boundary $\boldsymbol{L}$ point might be responsible for the observed first-order phase transition at ~8 GPa.

(Some figures in this article are in colour only in the electronic version)

1. Introduction

Binary intermetallic compounds AuX_2 (X = Al, Ga and In) that crystallize in the cubic fluorite (CaF_2) structure (space group, O_h^5 ($Fm3m$)) have received considerable attention, due to their fundamental and technological importance. These compounds are known to exhibit a striking variety of colors, ranging from the bright mauve color of $AuAl_2$ to the neutral appearance of $AuGa_2$ and the bluish shade of $AuIn_2$ [1]. Previous studies of the electrical properties of AuX_2 showed that they are good metallic conductors with ambient-temperature conductivities about one fifth compared to that of Cu [2]. These compounds are found to be unstable at high temperatures [3], and possess superconducting properties at low temperatures [4]. Moreover, they are the excellent systems for studying the transition-metal 5d bands.

[1] Author to whom any correspondence should be addressed.

Many experimental [5–23] and theoretical [19–28] explorations have been conducted to investigate the electronic, transport and dynamical properties of AuX_2 at ambient pressure. However, the high-pressure behaviors are less often reported in the literature. These intermetallic compounds undergo a number of electronic topological transitions (ETTs) and structural phase transitions under pressure [21–23]. Godwal *et al* [22] first observed the anomalies of resistance, thermoelectric power (TEP, Seebeck coefficient) and universal equation of state (UEOS) in $AuIn_2$ and demonstrated that there is an ETT occurring in the pressure range 2–4 GPa, while the imaging plate high-pressure angle-dispersive x-ray diffraction (ADXRD) data indicated a structural phase transition beyond 8 GPa to a monoclinic phase. Recently, however, Garg *et al* [21] excluded the possibility of the existence of an ETT in $AuAl_2$ from the evidence of a smooth change of the resistance and UEOS measurements with pressure. Also, the ADXRD data indicated that $AuAl_2$ undergoes a structural transition beyond 12 GPa to an orthorhombic phase. Very recently, Garg *et al* [23] performed measurements of resistance, TEP and UEOS, and suggested that there also exists a pressure-induced ETT near 3.2 GPa in $AuGa_2$. In synchrotron-based high-pressure x-ray diffraction measurements, the behavior of the diffraction lines from $AuGa_2$ implied a transition to a structure closely related to CaF_2 type by distortion at about 8 GPa [23]. On the theoretical side, there exist only electronic band structure calculations in AnX_2 and TEP measurements in $AuIn_2$ under pressure [21–23, 28]. In this paper, we present a comprehensive picture of the electronic and transport properties, and lattice dynamics in AuX_2 at ambient and high pressures.

An ETT takes place when doping, pressure, or other external agents modify the Fermi surface of an electronic system, with important consequences on its properties. An ETT of the first type with a change in topology of the spherical image of a Fermi surface is due to a change in the topology of the Fermi surface at some critical energy; the isoenergy surface contains singular points [29–31]. An ETT of the second type with a change in the topology of the spherical images of the Fermi surface is associated with an abrupt change in the local differential-geometric characteristics of the Fermi surface with no change in the topology of the surface; the isoenergy surface has no singular points [32]. In order to uncover the physical nature of the ETTs in $AuIn_2$ and $AuGa_2$, a detailed study of the band structure and Fermi surface under pressure in AuX_2 was performed.

It is known that the changes in the Fermi surface have a subtle effect on the transport properties. The TEP is related to the derivatives of the electronic density of states at the Fermi surface $N(E)$, and the band velocity $\upsilon_f(E)$, and therefore depends on the details of the electronic band structure. We have shown earlier, in the study of possible ETTs at high pressure in Nb [33] and Os [34], that the Hall coefficient related to the inverse of the effective mass, which is the second derivative of the band dispersion of the electronic bands near the Fermi surface, can be a very sensitive test for the change in electronic band structure [33]. Thus, we also investigate the interesting phenomenon of pressure-induced change of the TEP and Hall coefficient in AuX_2.

Furthermore, an ETT not only leads to unusual concentration dependences of the resistivity, TEP and Hall coefficient of the system but also other interesting phenomena such as lattice instability [35–41]. It is known that dynamic instabilities are often responsible for phase transitions under pressure. Meanwhile, the lattice dynamics plays an important role in understanding the different mechanisms of phase transitions. A connection between the ETT and a structural phase transition has been observed in Cs metal, which exhibits an isostructural (fcc–fcc; fcc stands for face-centered cubic) phase transition at room temperature between the two high-pressure modifications Cs(II) and Cs(III) [35–38]. In Cs metal, the ETT is found to be the precursor of the isostructural phase transition. At the ETT the electronic contribution to the internal pressure changes markedly and causes a softening of phonon modes which finally

leads to the isostructural transition. ETTs in hexagonal close-packed (hcp) Zn [39, 40] and Cd [41] under hydrostatic pressure and their influence on the low-frequency phonons of these metals have also been reported. In this study, lattice dynamics calculations show no phonon softening up to 12 GPa for both $AuAl_2$ and $AuIn_2$. At 22.4 GPa, the phonon frequencies of the TA modes decrease to be imaginary at the zone boundary $\boldsymbol{L}$ point in $AuGa_2$. Although this phase transition pressure is much higher than the experimental one, the 'mode-softening' behavior may be related to the particular mechanism that is responsible for the phase transition.

2. Computational details

The electronic band structure and Fermi surface of AuX_2 were mainly calculated by using the all-electron full potential linearized augmented plane wave (FP-LAPW) method with and without the consideration of spin–orbital (SO) coupling, as implemented in the WIEN2K [42] code within the framework of density-functional theory (DFT) [43]. The muffin-tin radii were chosen to be 2.3, 2.1, 2.1 and 2.2 au for Au, Al, Ga and In atoms, respectively. The local-density approximation (LDA) [44] was mainly employed. The cutoff angular momentum maximum ($l_{\max}$) for the wavefunction was confined to be $l_{\max} = 10$. The self-consistent field calculations were found to be well-converged with the choices of a 2000 k-point set and an energy cutoff of $RK_{\max} = 7$. The electronic band structure calculations were also performed using the pseudopotential plane wave (PP-PW) method, as implemented in the Quantum-ESPRESSO [46] and CASTEP [47] codes. The two-dimensional (2D) Fermi surface along the $\boldsymbol{\Gamma}$–$\boldsymbol{K}$–$\boldsymbol{X}$ plane was calculated using the FP-LAPW method with SO coupling. The transport properties were calculated by using the BoltzTraP [48] code, which relies on a well-tested smoothed Fourier interpolation to obtain an analytical expression of the bands. A much denser 100 000 k-point set was chosen in the transport calculation. The lattice dynamics with pressure were investigated using the PP-PW density-functional linear-response method [43], using the Quantum-ESPRESSO [46] code. As phonons are not sensitive to SO effects [49], the lattice dynamics calculations neglect the SO coupling. The Troulier–Martins [50] norm-conserving scheme was used to generate the pseudopotentials for Au, Al, Ga, and In with valence electron configurations of $5d^{10}6s^1$, $3s^23p^1$, $3d^{10}4s^23p^1$, and $4d^{10}5s^25p^1$ respectively. The convergence tests gave the kinetic energy cutoffs of 90 Ryd, 110 Ryd and 90 Ryd for $AuAl_2$, $AuGa_2$ and $AuIn_2$, respectively, with an $8 \times 8 \times 8$ Monkhorst–Pack (MP) grid for the electronic Brillouin zone (BZ) integration. A $4 \times 4 \times 4q$ mesh in the first BZ was used in the interpolation of force constants in the phonon calculations.

3. Results and discussion

The theoretical total energies as a function of volume were fitted to the Murnaghan equation of state [51] to obtain the theoretical equilibrium lattice parameter (a_0), bulk modulus (B_0) and the pressure derivative of the bulk modulus (B_0') as listed in table 1. The calculations were performed with both the LDA [44] and the generalized gradient approximation (GGA) [45] to estimate the accuracy of different choices of the exchange–correlation function. The experimental data [7, 21–23] are also listed for comparison. We note that the theoretical lattice parameters with and without the consideration of SO coupling are almost identical, and those values calculated by the LDA agree better with the experimental values than the GGA methods. In particular, with the PP-PW method, it is found that the lattice parameters of $AuGa_2$ and $AuIn_2$ calculated by the LDA are in excellent agreement with the experiment results, and it underestimates by only $\sim$1.17% in $AuAl_2$. However, the GGA overestimates the lattice parameters of $AuAl_2$, $AuGa_2$ and $AuIn_2$ by 0.67%, 1.32% and 1.23% respectively.

Table 1. Calculated equilibrium lattice parameter (a_0), bulk modulus (B_0) and the pressure derivative of bulk modulus (B_0') for AuX_2. The calculations including SO coupling are shown in curly brackets. Previous experimental results are also shown for comparison. The units for a_0 and B_0 are Å and Mbar, respectively.

Material	Method		a (Å)	B_0 (Mbar)	B_0'
$AuAl_2$	FP-LAPW	LDA	5.94{5.95}	1.22{1.46}	4.72{2.34}
		GGA	6.01{6.02}	1.08{1.31}	4.81{3.26}
	PP-PW	LDA	5.93	1.20	4.83
		GGA	6.04	1.03	4.49
	Exp.		6.0[a]	1.11[b]	4[b]
$AuGa_2$	FP-LAPW	LDA	6.00{6.01}	1.03{1.07}	7.08{6.79}
		GGA	6.18{6.18}	0.68{0.75}	6.28{5.91}
	PP-PW	LDA	6.09	0.88	5.53
		GGA	6.16	0.73	5.09
	Exp.		6.08[a]	0.98[c]	4[c]
$AuIn_2$	FP-LAPW	LDA	6.45{6.45}	0.78{0.77}	4.77{6.87}
		GGA	6.66{6.58}	0.62{0.84}	4.11{4.34}
	PP-PW	LDA	6.51	0.75	6.27
		GGA	6.59	0.58	5.77
	Exp.		6.51[a]	0.50[d]	4[d]

[a]Reference [7].
[b]Reference [21].
[c]Reference [23].
[d]Reference [22].

Furthermore, the LDA is known to describe 5d transition metals better than the GGA [52, 53]. Thus, we employed the LDA for the rest of the study. Note also that almost identical results in the band structure calculations were obtained by using the FP-LAPW and PP-PW methods, signifying the consistency of the choices of different methods.

To explore the ETT in AuX_2, the electronic band structures and Fermi surfaces with SO coupling were calculated using the FP-LAPW method. For comparison, the electronic band structures and Fermi surfaces obtained from calculations without SO coupling were also examined. The inclusion of SO coupling only results in a small splitting in the degenerate bands along the directions $\boldsymbol{L}$–$\boldsymbol{\Gamma}$ [$\xi\xi\xi$] and $\boldsymbol{\Gamma}$–$\boldsymbol{X}$ [ξ00] in the BZ. The gross features of the Fermi surfaces with and without the inclusion of SO coupling are essentially identical. This observation substantiates the validity of neglecting the SO coupling in the calculation of dynamical properties. As shown in figure 1, the band structures and 2D Fermi surfaces for $AuAl_2$ do not show any distinct changes at pressures of zero and 5 GPa, and there is no further noticeable change when the pressure increases up to 12 GPa (not shown). Therefore, the possibility of the existence of an ETT in $AuAl_2$ is excluded. This fact is in good agreement with the previous experimental and theoretical results [21].

Figure 2 shows the band structures and 2D Fermi surfaces at different pressures for $AuGa_2$. At zero pressure, as shown in figure 2(a), it is found that there is an energy band around the BZ boundary $\boldsymbol{X}$ point crossing the Fermi level in the middle of $\boldsymbol{\Delta}$ direction and near the $\boldsymbol{X}$ point along the $\boldsymbol{Z}$ direction, respectively, leaving a fully occupied flat band below the Fermi level. The reflection of the band structure features near the $\boldsymbol{X}$ point in the 2D Fermi surface plot is a half-ellipse-like hole, as depicted in figure 2(b). It is very interesting to note that with increasing pressure the energy band moves up; in particular, it has shifted over the Fermi level at the $\boldsymbol{X}$ point when the pressure increases up to 4 GPa. This intriguing band structure evolution results in a significant change of the Fermi surface topology around the $\boldsymbol{X}$ point, as shown

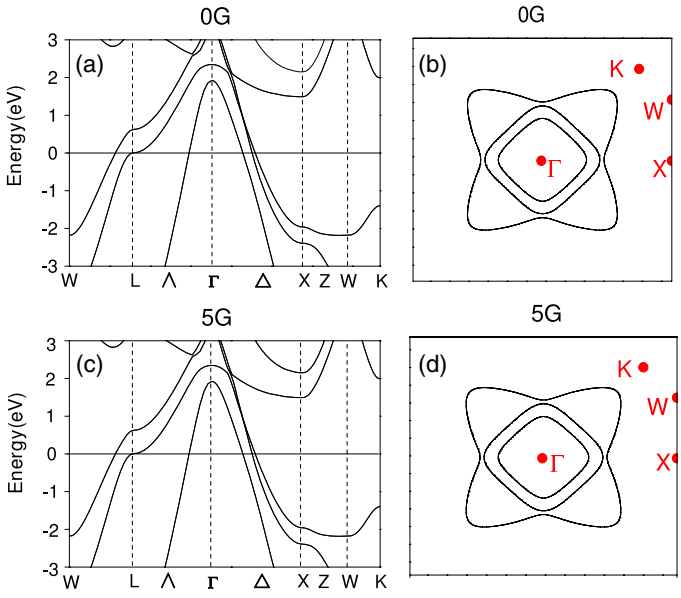

Figure 1. Calculated band structures and two-dimensional Fermi surfaces for $AuAl_2$ along several high-symmetry directions in the BZ at zero and 5 GPa.

in figure 2(d), signifying the occurrence of an ETT. The variation of band energy at the $\boldsymbol{X}$ point relative to the Fermi level with pressure is represented in figure 3. A transition pressure of ∼3.5 GPa for the predicted ETT is obtained, in good agreement with the experimentally observed ETT transition pressure near 3.2 GPa [23]. As the pressure increases up to 8 GPa, the whole energy band has moved over the Fermi level, as indicated in figure 2(e). As a consequence, the small hole along the $\boldsymbol{\Gamma}$–$\boldsymbol{X}$ [ξ00] direction in the 2D Fermi surface vanishes completely at 7.2 GPa (figure 3), as shown in figure 2(f). The current theoretical prediction might imply another ETT in $AuGa_2$ at ∼7.2 GPa which has not been experimentally reported.

Figure 4 shows the band structures and 2D Fermi surfaces at different pressures for $AuIn_2$. At zero pressure, the red colored band crossing over Fermi level at the $\boldsymbol{\Gamma}$ point along $\boldsymbol{L}$–$\boldsymbol{\Gamma}$–$\boldsymbol{X}$ direction is clearly predicted, as shown in figure 4(a). The current calculation is in good agreement with previous experimental result [17] and theoretical calculations [25–27]. However, it is in contrast to two other previous theoretical calculations by Godwal *et al* [22] and Gao *et al* [28]. Their calculations showed that the whole red band along $\boldsymbol{L}$–$\boldsymbol{\Gamma}$–$\boldsymbol{X}$ is fully occupied at the ambient pressure. Base on this fact, they further argued that the red band moved over Fermi level with pressure, and thus opened a pocket in the Fermi surface, which is attributable to the experimentally observed ETT. Therefore, to uncover the electronic origin of the ETT, it is crucial to clarify if the red band had already crossed the Fermi Level at the $\boldsymbol{\Gamma}$ point at zero pressure. As we described above, we indeed found the band-crossing feature at zero pressure to be supported by the experimental angle-resolved photoemission results [17] and three previously theoretical calculations [25–27]. Besides, we also performed additional calculations using the PP-PW method through Quantum-ESPRESSO [46] and CASTEP [47] codes with both GGA and LDA implementations. All the evidence strongly supported the validity of our results. We thus excluded the pressure-induced band crossing origin at the $\boldsymbol{\Gamma}$ point for the ETT. From figure 4, it is clear that there is no significant modification of the band structure under pressure, but one notices that two intersection points of the bands along

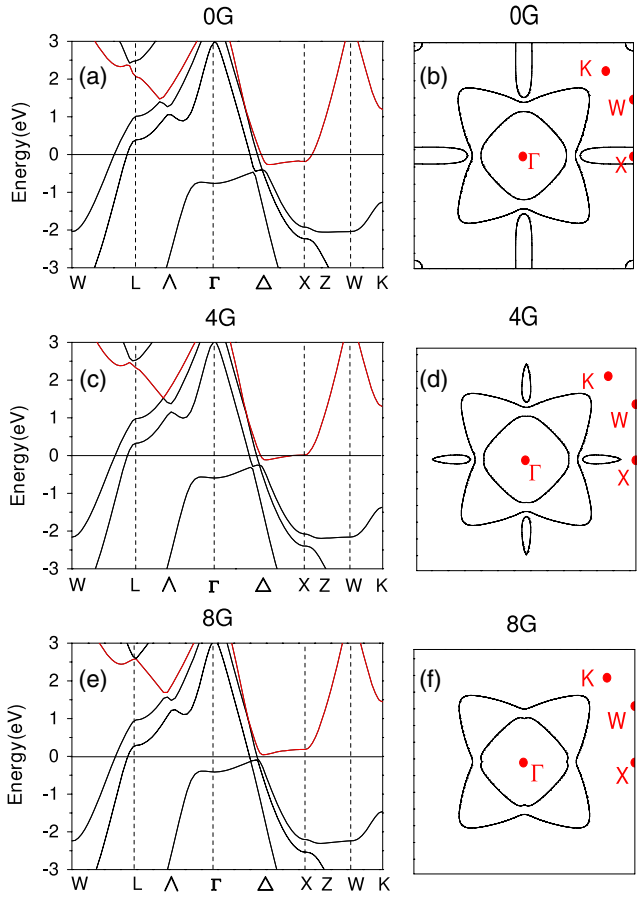

Figure 2. Calculated band structures and two-dimensional Fermi surfaces for $AuGa_2$ along several high-symmetry directions in the BZ at zero and 4 GPa.

the Γ–X [ξ00] direction have shifted over the Fermi level at ∼4 GPa. This fact results in an abrupt change in the geometric characteristic of the Fermi surface around the Γ point, as indicated in figure 4(d). The ETT the occurs in $AuIn_2$ might belong to a new type of ETT reported by Makarov *et al* [32] which is associated with an abrupt change in the local differential-geometric characteristics of the Fermi surface with no change in the topology of the surface. This geometric variation in the Fermi surface does not support a strong ETT in $AuIn_2$. It is noteworthy that the appearance of the abrupt change in the Fermi surface occurs at ∼3 GPa, which is in good agreement with the experimentally observed anomalies in the measured resistance and thermoelectric power in the pressure range 2–4 GPa [22].

The calculated TEP and Hall coefficient at 300 K of AuX_2 as a function of pressure are presented in figures 5(a) and (b), respectively. It is clear that the TEP of $AuAl_2$ changes slightly with pressure, as indicated by the solid squares in figure 5(a), whereas it changes dramatically with pressure in $AuGa_2$ and $AuIn_2$. Interestingly, the TEP in $AuGa_2$ increases more quickly beyond 1.5 GPa, changing its sign from negative to positive at ∼2 GPa, and it has an obvious 'kink' at ∼6 GPa. The theoretical trend is in qualitative agreement with experimental measurements [23]. For $AuIn_2$, the calculated TEP has noticeable small 'kink'

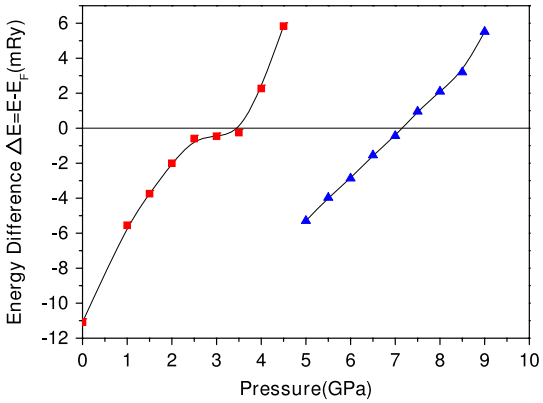

Figure 3. Energy differences of the bands form the Fermi energy at the high-symmetry point ***X*** on the first BZ boundary (red solid squares) and the lower-most point of the energy band along the **Γ**–***X*** direction (blue solid triangles) as a function of pressure for $AuGa_2$. Solid line through the calculated data points represents fitted curves using a B-spline.

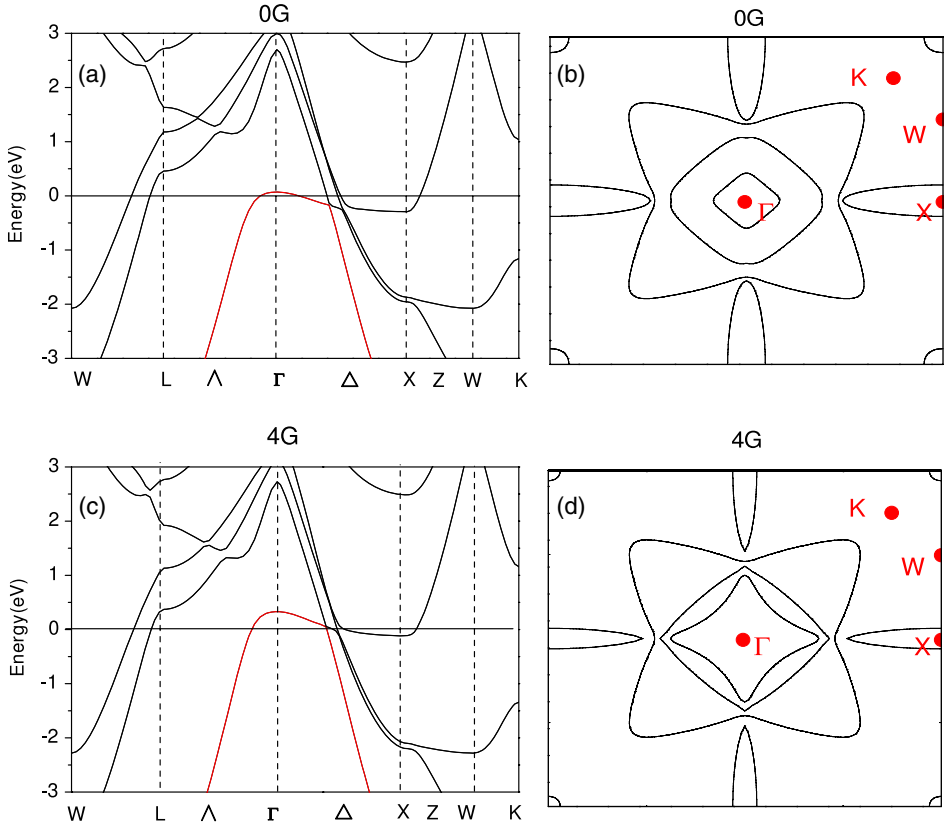

Figure 4. Calculated band structures and two-dimensional Fermi surfaces for $AuIn_2$ along several high-symmetry directions in the BZ at zero, 4 and 8 GPa.

at ∼1.5 GPa. The theoretical trend is also in qualitative agreement with the experimental results [22], and the values are in very good agreement with the calculations of Gao *et al* [28].

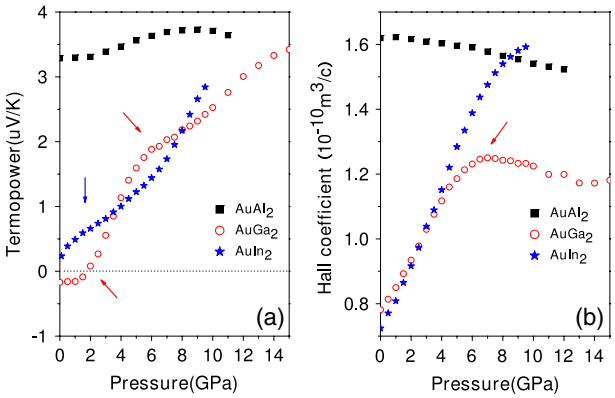

Figure 5. Calculated TEP and Hall coefficient as a function of pressure for AuX_2 with SO interaction.

However, the theoretical values for the TEP in $AuGa_2$ and $AuIn_2$ are both slightly lower than those observed in the experiments [22, 23]. The calculated TEPs are predicted to show two anomalies in $AuGa_2$ at ∼1.5 and ∼6 GPa, respectively, which are close to the ETT transition pressures of 3.5 GPa and 7.2 GPa; the anomaly in $AuIn_2$ occurs at 1.5 GPa, corresponding to the ETT transition pressure of 3.5 GPa. One observes that, as the pressure increases, the Hall coefficient of $AuAl_2$ decreases slightly, as plotted in figure 5(b), while in $AuIn_2$ the Hall coefficient increases sharply and does not exhibit any visible anomaly. However, it is important to note that the Hall coefficient of $AuGa_2$ reaches its maximum value at ∼7 GPa, but an expected anomaly in the pressure variation near 3.5 GPa is not seen in the calculation. The current calculations confirm that the anomalous transport behaviors of $AuGa_2$ and $AuIn_2$ are mainly due to the flat bands along the $\boldsymbol{\Gamma}$–$\boldsymbol{X}$ direction close to the Fermi level. This is particularly important for very flat bands, which are associated with high density of states and therefore large TEP and Hall coefficient [54]. The anomalous transport properties take place at a pressure in the range of pressures in which the ETT occurs; furthermore, the anomalies in the TEP and Hall coefficient are the result of the interplay of several electronic bands close to the Fermi level. Consequently, the occurrences of an anomaly in the TEP and Hall coefficient do not necessarily correspond exactly to the pressure at the ETT. It is clear that the ETT plays an important role in the anomalies of the TEP and Hall coefficient.

Figure 6 shows the calculated phonon dispersion curves and projected phonon density of states (DOS) for AuX_2 at zero pressure. As AuX_2 is a metallic crystal, the longitudinal optical (LO) and transverse optical (TO) phonon modes are triply degenerate at the $\boldsymbol{\Gamma}$ point, as expected. The two irreducible representations for the optical modes are $\Gamma(O_h^5) = F_{1u} + F_{2g}$, where F_{1u} is infrared active while F_{2g} is Raman active. The calculated phonon modes at the zone center are listed in table 2. The experimental Raman data [10, 11] and previous calculations [24, 27] are also listed for comparison. It is clear that the current calculations are in excellent agreement with experimental measurements and previous theoretical predictions. From the projected phonon DOS plot as shown in figure 6(b), it is found that there is only small coupling between Au and Al vibrations due to the large difference (∼170) in their atomic mass, and Au atomic vibrations contribute mainly to the low-frequency acoustic phonons because of its larger atomic mass. With the decrease of the difference in the atomic mass, the vibration couplings between Au and Ga atoms, and between Au and In atoms, become increasingly stronger, as evidenced from figures 6(d) and (f), respectively. As a result, for $AuIn_2$, there is

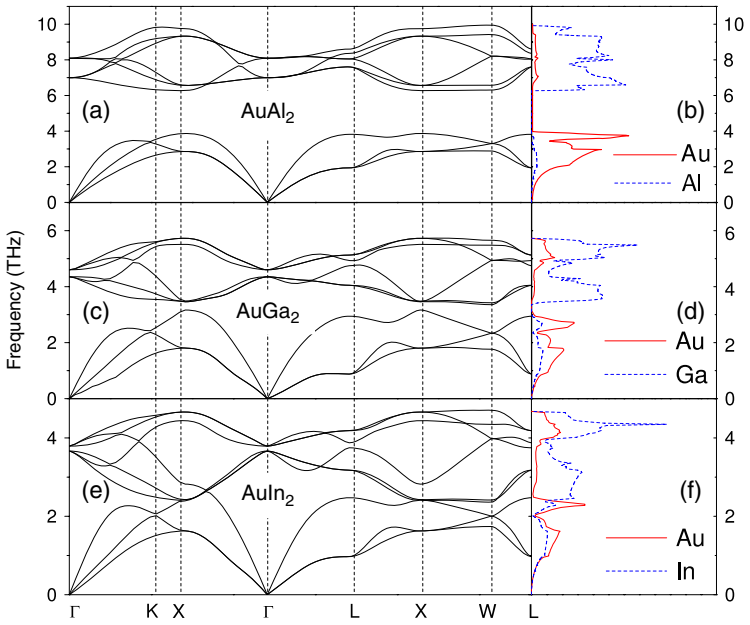

Figure 6. The calculated phonon frequencies and projected phonon DOS of AuX_2 at ambient pressure.

Table 2. Calculated phonon frequencies (in cm^{-1}) for AuX_2 at the zone center. Available theoretical calculations and experimental Raman scattering data at $T = 300$ K are also shown for comparison.

Material	Method	F_{1u}-LO (Raman)	F_{2g}-TO (IR)
$AuAl_2$	This work	270.0	233.4
	Reference [27]	268	231
	Exp.	267[a]{266[b]}	
$AuGa_2$	This work	153.3	144.7
	Reference [24]	148	142[b]
	Exp.	149[a]	
$AuIn_2$	This work	126.6	122.4
	Reference [24]	121	115
	Exp.	124[c]	

[a]Reference [10].
[b]Reference [11].

no clear gap between optical and acoustic phonons observed with the smallest mass difference of 82.

With increasing pressure, the phonon frequencies of $AuAl_2$ and $AuIn_2$ are predicted to show positive pressure dependence, as illustrated in the phonon DOS plots of figures 7(a) and (b), respectively. However, $AuGa_2$ exhibits different dynamics behavior with pressure. The calculated phonon dispersion curves of $AuGa_2$ and the projected phonon DOS at different pressures are shown in figure 8. One observes that with increasing pressure (decreasing volume), the TO, LO, and longitudinal acoustic (LA) phonon modes shift to higher frequencies, while the transverse acoustic (TA) phonon branch along the $\mathbf{\Gamma}$–$\boldsymbol{L}$ $[\xi\xi\xi]$ direction decreases in frequency, indicating a negative mode Grüneisen parameter, $\gamma_j(q) = -\partial \ln \upsilon_j(q)/\partial \ln V$ for

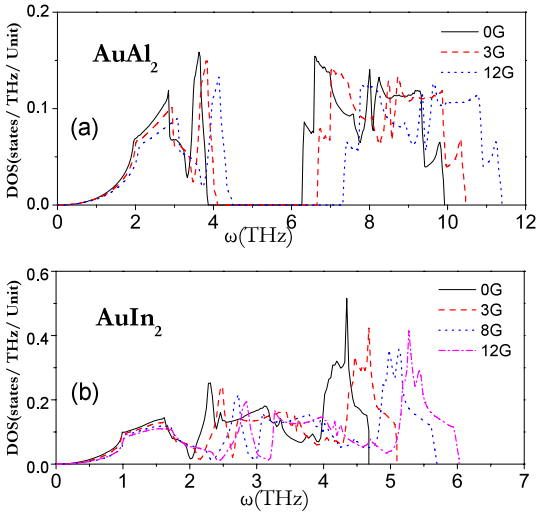

Figure 7. The theoretical phonon density of states at various pressures for $AuAl_2$, and $AuIn_2$.

mode j, where q is the wavevector, ν is the frequency, and V is the volume. At a volume of 0.857 V_0 the phonon frequencies of the TA modes along the Γ–L [$\xi\xi\xi$] direction decrease to be imaginary, signaling a structural instability in the fluorite phase. Figure 9 shows the variation of the frequency of the TA (q) mode for the most negative L (0.5 0.5 0.5) point in figure 8(e) with pressure. The squared phonon frequencies ν^2 for the TA branch at the L (0.5 0.5 0.5) point with pressure P are also plotted as shown in the inset of figure 9. A near-perfect linear relation between ν^2 and P is obtained. The estimated transition pressure is ∼22.4 GPa ($V = 0.853\ V_0$) from figure 9. Such behavior is consistent with the Landau theory of pressure-induced soft-mode phase transitions. Phonon softening usually corresponds to the instability of a particular atomic movement. The calculated transition pressure, 22.4 GPa, is much higher than the experimental transition pressure, ∼8 GPa, at room temperature, even if one allows for the temperature effects. This big difference indicates that the phase transition may not be induced independently by the phonon instability at the zone boundary L point. This behavior of the phonon softening to zero frequency is hidden by the first-order transition. Although this phase transition occurs at pressures far below those required to drive the TA modes to zero frequency, the 'mode-softening' behavior may be related to the particular mechanism that is responsible for the phase transition.

4. Conclusion

In summary, we have presented a comprehensive picture of the electronic properties, transport properties, and lattice dynamics in AuX_2 at ambient pressure and high pressure. The calculations of electronic band structures and 2D Fermi surfaces reveal a pressure-induced ETT in $AuGa_2$ and $AuIn_2$, while it is absent for $AuAl_2$. The ETT in $AuIn_2$ is predicated to be related to an abrupt change in the local differential-geometric characteristics of the Fermi surface at ∼3 GPa. In $AuGa_2$, the ETT is identified with a change in the Fermi surface topology of the X point at ∼3.5 GPa due to the energy band crossover of the Fermi level. As the pressure increases, we predicted a new ETT in $AuGa_2$ at ∼7.2 GPa resulting from a topological singularity along the Γ–X [ξ00] direction of the Fermi surface which has not been

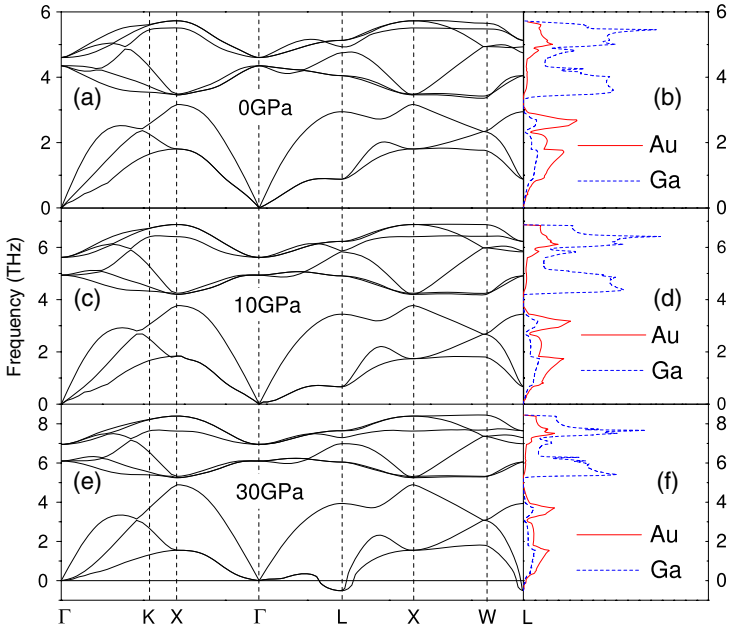

Figure 8. Calculated phonon frequencies and projected phonon DOS for $AuGa_2$ at different pressures.

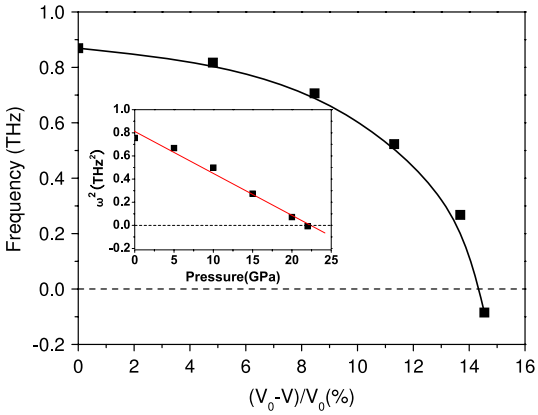

Figure 9. Calculated TA phonon frequencies at the $\boldsymbol{L}$ point of the BZ in $AuGa_2$ as a function of volume. The solid line through the calculated data points represents fitted curves using a B-spline. Inset: the calculated squared phonon frequency ω^2 as a function of pressure. The solid line through the data points is a linear fit.

experimentally reported. The ETT plays an important role in the anomalies of the TEP and Hall coefficient. No unusual softening in the phonon dispersions was observed in $AuAl_2$ and $AuIn_2$ up to 12 GPa. Interestingly, a TA phonon branch softens to zero frequency at the BZ boundary $\boldsymbol{L}$ point in $AuGa_2$, and it may induce the first phase transition to the orthorhombic phase.

Besides the ETT, transport and lattice dynamical properties, there are many properties of the three compounds that are different from each other. Specifically, the properties such as the de Haas–van-Alphen orbits, F_1 and F_2 in the notation of [5], are unique to $AuAl_2$. $AuGa_2$ is

different from the other two in terms of anomalous thermoelectric power, elastic constants [55] and Knight shift [4, 6]. Earlier investigations into the variation of melting point with pressure on AuX_2 reveal that it decreases with pressure for $AuAl_2$ and $AuGa_2$, while for $AuIn_2$ it remains constant to about 3 GPa and then acquires a position slope at higher pressures nearing 5 GPa [3]. Therefore, further research works are needed to clarify the physics behind the above intriguing features in AuX_2.

Acknowledgments

We are grateful for the financial support of the China 973 Program under grant no. 2005CB724400, the NSAF of China under Grant no. 10676011, the National Doctoral Foundation of China Education Ministry under Grant no. 20050183062, the SRF for ROCS, SEM, the 2005 Program for New Century Excellent Talents in University, and the 2006 Project for Scientific and Technical Development of Jilin Province. Most of the calculations in this work have been done using the WIEN2k, BoltzTraP, Quantum-ESPRESSO and CASTEP packages.

References

[1] Zintl E, Harder A and Haucke W 1937 *Z. Phys. Chem. Abt.* B **35** 354
[2] Jan J-P and Pearson W B 1963 *Phil. Mag.* **8** 279
[3] Strom A R, Wernick J H and Jayaraman A 1966 *J. Phys. Chem. Solids* **27** 1227
[4] Wernick J H, Menth A, Geballe T H, Hull G and Maita J P 1969 *J. Phys. Chem. Solids* **30** 1949
[5] Jan J-P, Pearson W B, Saito Y, Springford M and Templton I M 1965 *Phil. Mag.* **12** 1271
[6] Jaccarino V, Weber M, Wernick J H and Menth A 1968 *Phys. Rev. Lett.* **21** 1811
[7] Hsu L-S 1994 *Mod. Phys. Lett.* B **8** 1297
[8] Testardi L R 1970 *Phys. Rev.* B **1** 4851
[9] Nelson J G, Gignac W J, Sehun K, Jeffrey R L and Williams R S 1984 *Phys. Rev.* B **31** 3649
[10] Brya W J 1971 *Solid State Commun.* **9** 2271
[11] Feldman D W, Parker J H Jr and Ashkin M 1968 *Phys. Rev. Lett.* **21** 607
[12] Sham T K, Perlman M L and Watson R E 1979 *Phys. Rev.* B **19** 539
[13] Perez I, Qi B, Liang G, Lu F, Croft M and Wieliczka D 1988 *Phys. Rev.* B **38** 12233
[14] Nelson J G, Gignac W, Kim J S, Lince J R and Williams R S 1985 *Phys. Rev.* B **31** 3469
[15] Hsu L S, Uo G Y, Denlinger J D and Allen J W 2001 *J. Phys. Chem. Solids* **62** 1047
[16] Hsu L S, Huang H-W and Tsang K-L 1998 *J. Phys. Chem. Solids* **59** 1205
[17] Schirber J E 1972 *Phys. Rev. Lett.* **24** 1127
[18] Jaccarino V, Weger M, Wernick J H and Menth A 1968 *Phys. Rev. Lett.* **21** 1811
[19] Kim K J, Harmon B N, Chen L-Y and Lynch D W 1990 *Phys. Rev.* B **42** 8813
[20] Hsu L S, Wang Y K, Tai Y L and Lee J F 2005 *Phys. Rev.* B **72** 115115
[21] Garg A B, Verma A K, Vijayakumar V, Rao R S and Godwal B K 2005 *Phys. Rev.* B **72** 024112
[22] Godwal B K, Jayaraman A, Meenakshi S, Rao R S, Sikka S K and Vijayakumar V 1998 *Phys. Rev.* B **57** 773
[23] Garg A B, Verma A K, Vijayakumar V, Rao R S and Godwal B K 2006 *J. Phys.: Condens. Matter* **18** 8523
[24] Uğur G and Soyalp F 2006 *J. Phys.: Condens. Matter* **18** 6777
[25] Kim S, Nelso J G and Williams R S 1985 *Phys. Rev.* B **31** 3460
[26] Switendick A C and Narath A 1969 *Phys. Rev. Lett.* **22** 1423
[27] Tütüncü H M, Altuntas H, Srivastava G P and Uğur G 2004 *Phys. Status Solidi* c **1** 3027
[28] Gao X, Uehara K, Klug D D, Patchkovshii S, Tse J S and Tritt T M 2005 *Phys. Rev.* B **72** 125202
[29] Lifshitz I M 1960 *Zh. Eksp. Teor. Fiz.* **38** 1569
[30] Phillips J C 1956 *Phys. Rev.* **104** 1263
[31] Hove L V 1953 *Phys. Rev.* **89** 1189
[32] Makarov V I, Bolotov D V, Gor'kavyĭ V A and Yatsenko A A 2005 *Low Temp. Phys.* **31** 321
[33] Tse J S, Li Z Q, Uehara K, Ma Y M and Ahuja R 2004 *Phys. Rev.* B **69** 132101
[34] Ma Y M, Cui T, Zhang L J, Xie Y, Zou G T, Tse J S, Gao X and Klug D D 2005 *Phys. Rev.* B **72** 174103
[35] Glötzel D and Mcmahan A K 1979 *Phys. Rev.* B **20** 3210

[36] Kennedy G C, Jayaraman A and Newton R C 1962 *Phys. Rev.* **126** 1363
[37] McMahan A K 1978 *Phys. Rev.* B **17** 1521
[38] Boehler R and Ross M 1984 *Phys. Rev.* B **29** 3673
[39] Li Z Q and Tse J S 2000 *Phys. Rev. Lett.* **85** 5130
[40] Steiner M, Polzel W, Karzel H, Schiessl W, Köfferlein M, Kalvius G M and Blaha P 1996 *J. Phys.: Condens. Matter* **8** 3581
[41] Yu K, Pushkarev V V and Holse A 1983 *Zh. Eksp. Teor. Fiz* **84** 1494
[42] Blaha P, Schwarz K, Madsen G K H, Kvasnicka D and Luitz J 2001 *WIEN2K: An Augmented Plane Wave plus Local Orbitals Program for Calculating Crystal Properties* (Vienna: Technische Universität Wien) ISBN 3-9501031-1-2
[43] Baroni S, Giannozzi P and Testa A 1987 *Phys. Rev. Lett.* **58** 1861
Giannozzi P, Gironcoli S D, Pavone P and Baroni S 1991 *Phys. Rev.* B **43** 7231
[44] Perdew J P and Wang Y 1992 *Phys. Rev.* B **45** 13244
[45] Perdew J P, Burke K and Ernzerhof M 1996 *Phys. Rev. Lett.* **77** 3865
[46] Baroni S, Corso S D, Gironcoli S D and Giannozzi P http://www.pwscf.org
[47] Segall M D, Lindan P J D, Probert M J, Pickard C J, Hasnip P J, Clark S J and Payne M C 2002 *J. Phys.: Condens. Matter* **14** 2717
[48] Madsen G K H and Singh D J 2006 *Comput. Phys. Commun.* **175** 67
[49] Savrasov S Y 2000 *Linear-Response LMTO Programs PHN User's Manual* http://www.fkf.mpg.de/andersen/LMTOMAN/phnman.pdf
[50] Hennion B, Moussa F, Prevot B, Carabatos C and Schawb C 1972 *Phys. Rev. Lett.* **28** 964
[51] Murnaghan F D 1944 *Proc. Natl Acad. Sci. USA* **30** 244
[52] Yang Z, Wu R, Zhang Q and Goodman D W 2002 *Phys. Rev.* B **65** 155407
[53] Koerling M and Haeglund J 1991 *Phys. Rev.* B **45** 13293
[54] Uehara K and Tse J S 2000 *Phys. Rev.* B **61** 1639
[55] Testardi L R 1970 *Phys. Rev.* B **1** 4851